Supplemental Information: Remotely sensing river greenhouse gas exchange velocity using the SWOT satellite

Craig B Brinkerhoff[1,*], Colin J Gleason[1], Christopher J Zappa[2], Peter A Raymond[3], and Merritt H Harlan[1]

[1] Department of Civil & Environmental Engineering, University of Massachusetts, Amherst, MA
[2] Lamont-Doherty Earth Observatory, Columbia University, Palisades, NY
[3] School of the Environment, Yale University, New Haven, CT

[*] Correspondence: Craig B Brinkerhoff <cbrinkerhoff@umass.edu>

Contents

This supplementary information contains 5 texts, 5 figures and 2 tables.

Test S1: Estimating how hydraulically wide SWOT rivers are

To quantify the prevalence of hydraulically-wide, SWOT-observable rivers, we used the dataset of field-measured river hydraulics outlined in Section 2.1. That dataset has over 500,000 discrete measurements of river width, velocity, area, and discharge that were made by the United States Geological Survey (USGS) to calibrate streamgauge rating curves. Here, we describe how this dataset was filtered down to 22452 SWOT-observable rivers.

First, we removed all measurements tagged by the USGS as 'poor', measurements with non-finite values, or measurements of 0. While this would indicate a dry channel, our hydraulic geometry model necessitates within-bank flow. Likewise, because hydraulic geometry only applies to within-bank flows and not flood events, we remove all overbank flows. This was done by first filtering for sites with at least 20 measurements (to build robust estimates of bankfull hydraulics) and then calculating bankfull width and depth as the width or depth with a return period

23   of two years. While the only true way to calculate bankfull hydraulics is manually in the field, this

24   is obviously impractical here. A two-year return period is a standard approximation for

25   determining out-of-bank flow in single-channel meandering rivers and was the method used by

26   Brinkerhoff et al. (2019). We then removed all measurements with a width or depth beyond their

27   respective at-a-station 2 year values.

28   Finally, we filtered this dataset to only measurements at least 100m wide ('SWOT-

29   observable'). This left us with 22452 total river hydraulics measurements.

30   **Text S2: Gas exchange model derivations**

31   In this text we provide the full algebra to arrive at the four physically-based gas exchange

32   models we tested in this study. Consult Appendix A for all variable definitions. Note that α and β

33   are statistical parameters obtained via least squares regression for the small-eddy and Reynolds-

34   extension models, respectively. Subscripts denote variants of the same parameter, depending on

35   which ϵ model is employed (see Main Text).

36   **Small-eddy models (Equation 3 from Main Test)**

37   *Log-law-of-the-wall model for the turbulent dissipation rate (assume $\epsilon = \epsilon_S$)*

38
$$k_{600} = \alpha (\epsilon_S)^{1/4} \textbf{(S1)}$$

39
$$k_{600} = \alpha \left(\frac{U_*^3}{H} \right)^{1/4} \textbf{(S2)}$$

40
$$k_{600} = \alpha \left(\frac{\sqrt{gR_hS}^3}{H} \right)^{1/4} \quad \textbf{(S3)}$$

41
$$k_{600} = \alpha \left(\frac{(gHS)^{3/2}}{H} \right)^{1/4} \quad \textbf{(S4)}$$

42
$$k_{600} = \alpha(gS)^{3/8} H^{1/8} \textbf{(S5)}$$

43
Form-drag model for the turbulent dissipation rate (assume $\epsilon = \epsilon_D$)

44
$$k_{600} = \alpha_1 (\epsilon_D)^{1/4} \textbf{(S6)}$$

45
$$k_{600} = \alpha_1 (gS\bar{U})^{1/4} \textbf{(S7)}$$

46
Reynolds extension models (Equation 4 from Main Text)

47
Log-law-of-the-wall model for the turbulent dissipation rate (assume $\epsilon = \epsilon_S$)

48
$$k_{600} = \beta(\epsilon_S)^{1/4} A_p^{3/4} \textbf{(S8)}$$

49
$$k_{600} = \beta \left(\frac{U_*^3}{H} \right)^{1/4} \left((U_*H)^{1/2} \right)^{3/4} \textbf{(S9)}$$

50
$$k_{600} = \beta U_*^{9/8} H^{1/8} \textbf{(S10)}$$

51
$$k_{600} = \beta(gR_hS)^{9/16} H^{1/8} \textbf{(S11)}$$

52
$$k_{600} = \beta(gHS)^{9/16} H^{1/8} \textbf{(S12)}$$

53
$$k_{600} = \beta(gS)^{9/16} H^{11/16} \textbf{(S13)}$$

54 *Form-drag model for the turbulent dissipation rate (assume $\epsilon = \epsilon_D$)*

$$k_{600} = \beta_1(\epsilon_D)^{1/4}A_p^{3/4} \textbf{(S14)}$$

55

$$k_{600} = \beta_1(gS\bar{U})^{1/4}\big((U_*H)^{1/2}\big)^{3/4} \textbf{(S15)}$$

56

$$k_{600} = \beta_1(gS\bar{U})^{1/4}(gR_hS)^{3/16}H^{3/8} \textbf{(S16)}$$

57

$$k_{600} = \beta_1(gS\bar{U})^{1/4}(gHS)^{3/16}H^{3/8} \textbf{(S17)}$$

58

$$k_{600} = \beta_1(gS)^{7/16}\bar{U}^{1/4}H^{9/16} \textbf{(S18)}$$

59

60 **Text S3: BIKER hyperparameterization**

61   In this text we explain in detail how BIKER's prior distributions were determined for a

62 given river.

63   Prior distributions are defined by their hyperparameters. For BIKER, prior distributions are

64 formalized as truncated normal distributions of the log-transformed terms such that $log(X) \sim$

65 $\mathcal{N}(\mu, \sigma^2)$ for $\lambda < log(X) < \gamma$, using prior hyperparameters mean (μ), standard deviation (σ), and

66 upper (γ) and lower bounds (λ) for any parameter X. It is important to again stress, as we do in the

67 Main Text, that BIKER prior hyperparameters are described using only SWOT data to be

68 completely globally implementable. This use of the data to describe the priors is analogous to the

69 'empirical Bayes method' (Hoff, 2009).

70   A_{0_i} and n_i prior hyperparameters were assigned following Brinkerhoff et al. (2020). They

71 developed a set of river channel prior hyperparameters for McFLI algorithms that are entirely RS-

4

72 able and reflect differential channel hydraulics as a function of river geomorphology. They used

73 an extensive database of field measurements and statistical learning to identify patterns that

74 associate river width with the hydraulic priors needed to run McFLIs so that prior hyperparameters

75 are assigned to rivers using only the remotely sensed measurements. For this study, we extracted

76 A_{0_λ} and A_{0_γ} as the 5th and 95th percentile values rather than the absolute maximum and minimum

77 values to avoid physically impossible bounds on A_0.

78   This leaves the k_{600_t} hyperparameters to be defined. k_{600_μ} is set by invoking the hydraulic

79 geometry (HG) relationships described in Section 3.2.3 of the main text and Table S2 using the

80 data from Brinkerhoff et al. (2019). We replaced both depth and velocity terms from our gas

81 exchange model (Equation 7 in the Main Text) with these HG models, resulting in Equation S19

82 where Q is the mass-conserved streamflow for the river reach.

83
$$k_{600_\mu} = 62.82\left(gS_{i,t}\right)^{7/16}(0.252Q^{0.388})^{9/16} * (0.276Q^{0.164})^{1/4} \textbf{(S19)}$$

84   Obviously, we have no a priori information about Q. So, we use the Q prior that will be

85 globally available when SWOT launches: a mean annual estimate from a water balance model.

86 This is the standard prior information used to benchmark the SWOT discharge algroithms and is

87 provided with the simulated SWOT data by both Durand et al. (2016) and Frasson et al. (2021).

88 Using a temporally-invariant estimate of streamflow is the worst case scenario and BIKER's

89 performance will improve with a more informed prior on streamflow (and therefore k_{600}).

90 However as noted in the Main Text, our primary goal with this initial validation is to benchmark

91 BIKER's worst case scenario for performance and so we do that here.

92   k_{600_σ} is set to 0.30 (log-space). This corresponds to a coefficient of variation of

93   approximately 30%, which we took to reflect a reasonably strong agreement between the prior and

94   the observed values. k_{600_λ} was set to log(0.001) m/day. k_{600_γ} was set to log(500) m/day.

95   **Text S4: Determining complete BIKER model uncertainty**

96   Recall that $\sigma_{k_{600}}$ refers to the total uncertainty inherent in Equation 9, i.e. stemming from

97   the Reynolds-extension model (Equation 7) and Manning's equation for $\bar{U}$. For the purposes of

98   this study, we are validating BIKER against Equation 7 in the main text and so all uncertainties

99   associated with the β_1 parameter are ignored and we only need to reflect the Manning's uncertainty

100   in our specification of $\sigma_{k_{600}}^2$. Therefore, we take Hagemann et al. (2017)'s estimated uncertainty

101   from Manning's equation to infer streamflow from SWOT observations (0.25) and inflate it

102   slightly to also account for the hydraulically-wide channel assumption and arrive at 0.30. This is

103   the $\sigma_{k_{600}}$ used in this study.

104   In the scenario that BIKER is run on real SWOT data, $\sigma_{k_{600}}$ must reflect the full uncertainty

105   implicit in Equation 9 in the main text. This means we must also account for uncertainty from the

106   β_1 parameter. Assuming perfect, no-error measurements are made by the SWOT satellite, the full

107   Equation 7 uncertainty is expressed for some set of hydraulic observations as Equation S20. To

108   quantify total uncertainty in k_{600}, we push Monte Carlo simulations through Equation S20 and

109   take the mean uncertainty as a reasonable value for $\sigma_{k_{600}}$ once SWOT launches.

110   More specifically, we use the 166 hydraulically-wide measurements in our field-measured

111   k_{600} dataset (Section 2 in the Main Text) and push 166 different Monte Carlo simulations through

112   Equation S20. Note that each Monte Carlo simulation is itself 10,000 runs in order to obtain a

113   distribution of k_{600} estimates. For each of the 166 distributions of estimated k_{600}, we extract the

114   standard deviation as the uncertainty. We then take the average of those standard deviations to be

115   a reasonable estimate of $\sigma_{k_{600}}$. This ultimately provided a value of 1.1 for the log-transformed

116   $\sigma_{k_{600}}$ and should be used when running BIKER on real SWOT data.

117   $$log_{k_{600}} \sim \mathcal{N}\big[log(\beta_1), log(\sigma_{\beta_1})\big] + \frac{1}{4}\mathcal{N}\big[log(\bar{U}), log(\sigma_{mannings})\big]\frac{7}{16}log(gS) + \frac{9}{16}log(H) \textbf{(S20)}$$

118   **Text S5: Literature CO_2 flux models**

119   Here, we describe in more detail the three CO_2 flux models used to compare against BIKER

120   in Section 3.2.3. The specific equations used are outlined in Table S2.

121   In brief, gas fluxes (FCO_2) are only obtainable at the global scale via predictive equations

122   for k_{CO_2} per Equation 2. Here, we obtain FCO_2 using the in situ CO_2 data described in Section 3.1

123   and k_{CO_2} estimates. The k_{CO_2} estimates are calculated using Equation 7. Equation 7 is calculated

124   using 1) in situ streamflow data, and 2) hydraulic scaling equations from the literature that predict

125   river velocity and depth from streamflow. Specifically, these literature equations are the 'Raymond

126   2012', 'Raymond 2013', and 'Brinkerhoff 2019' models (Table S2).

127   For example, the 'Raymond 2012' model uses the hydraulic scaling equations from

128   Raymond et al. (2012) to predict velocity and depth, which are in turn used to calculate a k_{CO_2} via

129   equation 7, which finally is used to calculate FCO_2 via equation 1. Similarly, the 'Raymond 2013'

130   model uses the equations outlined in Raymond et al. (2013) and the 'Brinkerhoff 2019' model uses

131   new equations fit to the hydraulics dataset from Brinkerhoff et al. (2019) after the filtering

132   described in Text S1. We chose to include the 'Brinkerhoff 2019' model as the training dataset is

133   far larger than those used in either of the previous two models (Table S3: 104,624 versus 10,837

134   versus 1,026, respectively). Finally, we converted from k_{600} to k_{CO_2} following Raymond et al.
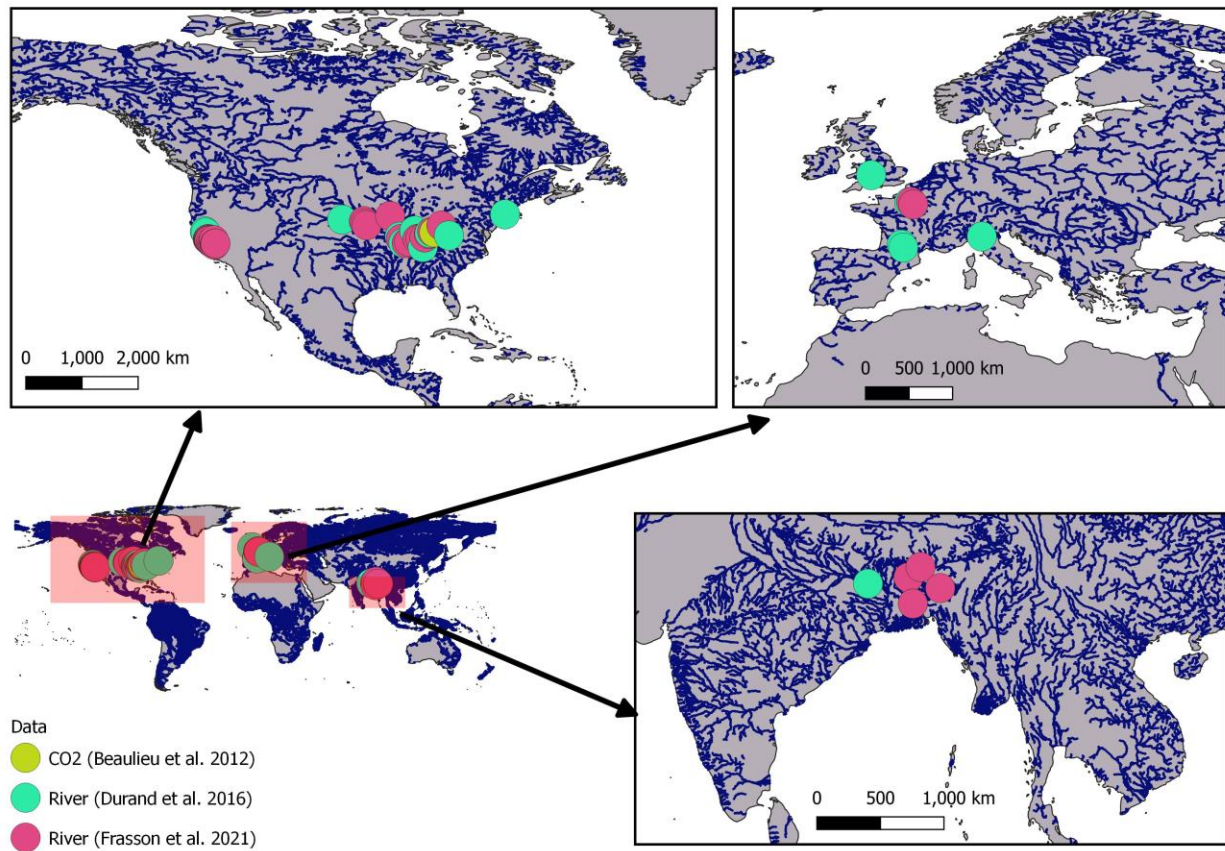
135   (2012).

136   **Figure S1**
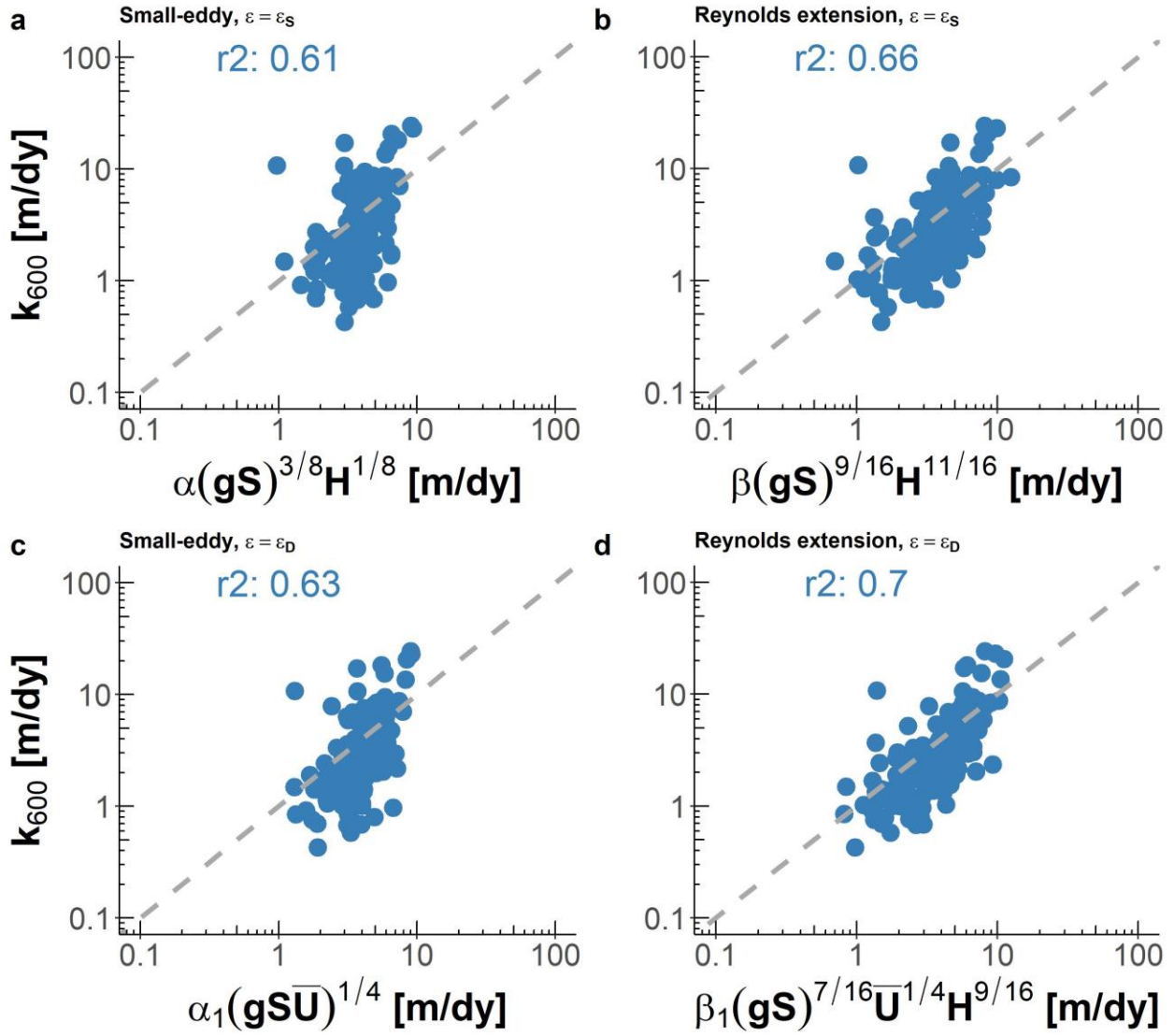
137

138   *Figure S1: Four k_{600}~hydraulics models tested in this study, with model assumptions noted*

139   *in the sub-panel titles. Panel (d) is also presented in the main text as Figure 2 and Equation 7.*
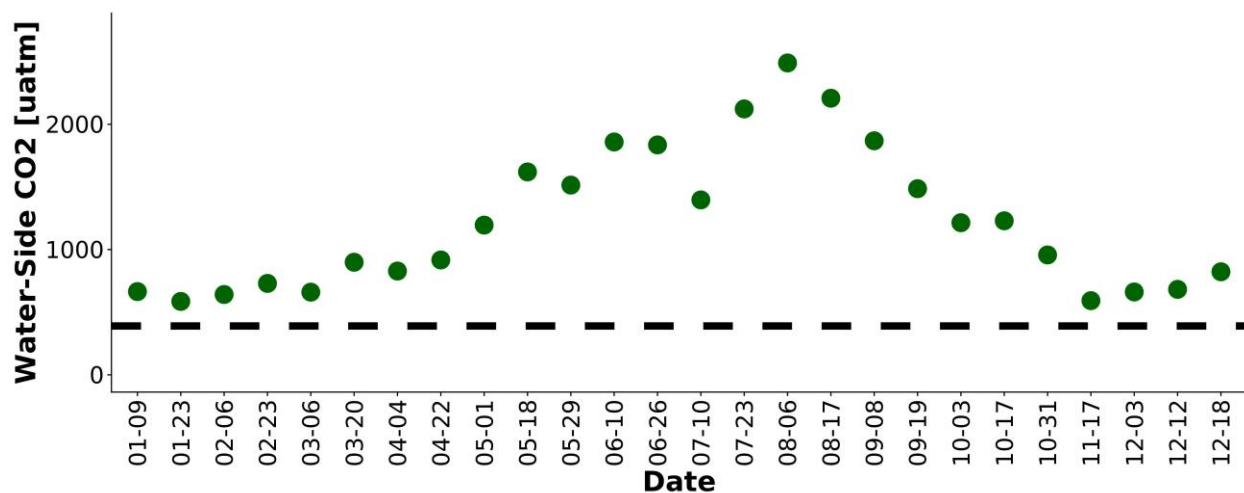
Figure S2

142   *Figure S2: Map of simulated SWOT river locations along the global SWOT river network*

143 *(Altenau et al., 2021). This corresponds to every river that BIKER could be run on once SWOT*

144 *launches. Also includes approximate location of the CO_2 timeseries used in this study (Figure S3).*

145 *Note that river locations are approximate as some hydraulic models are not geo-referenced.*

146   **Figure S3**

147

148   *Figure S3 Timeseries of the biweekly CO_2 data from Beaulieu et al. (2012). Sampling took*

149   *place 2008-2009 in the Ohio River (upstream of Cincinnati, Ohio, United States). Dashed black*
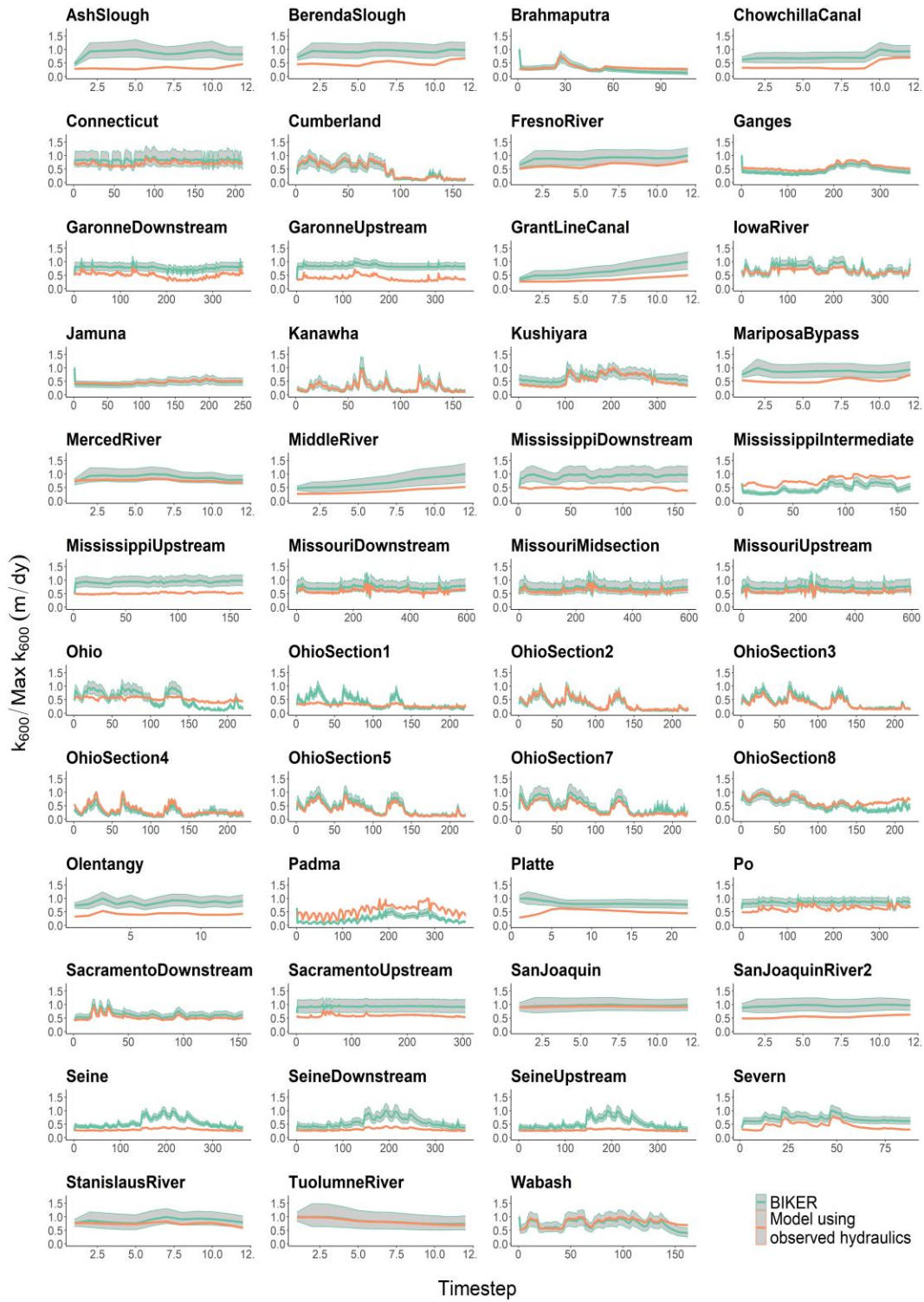
150   *line denotes atmospheric CO_2 at 400 uatm.*

Figure S4

Timestep

153   *Figure S4: Observed (orange) versus BIKER-inferred (green) timeseries of daily k_{600} for*

154   *the 47 SWOT-simulated rivers under the 'no-measurement-error' scenario. Green ribbon is*

155   *BIKER posterior 95% confidence intervals. Note that the y axis is normalized by maximum*

156   *observed values to compare across rivers.*
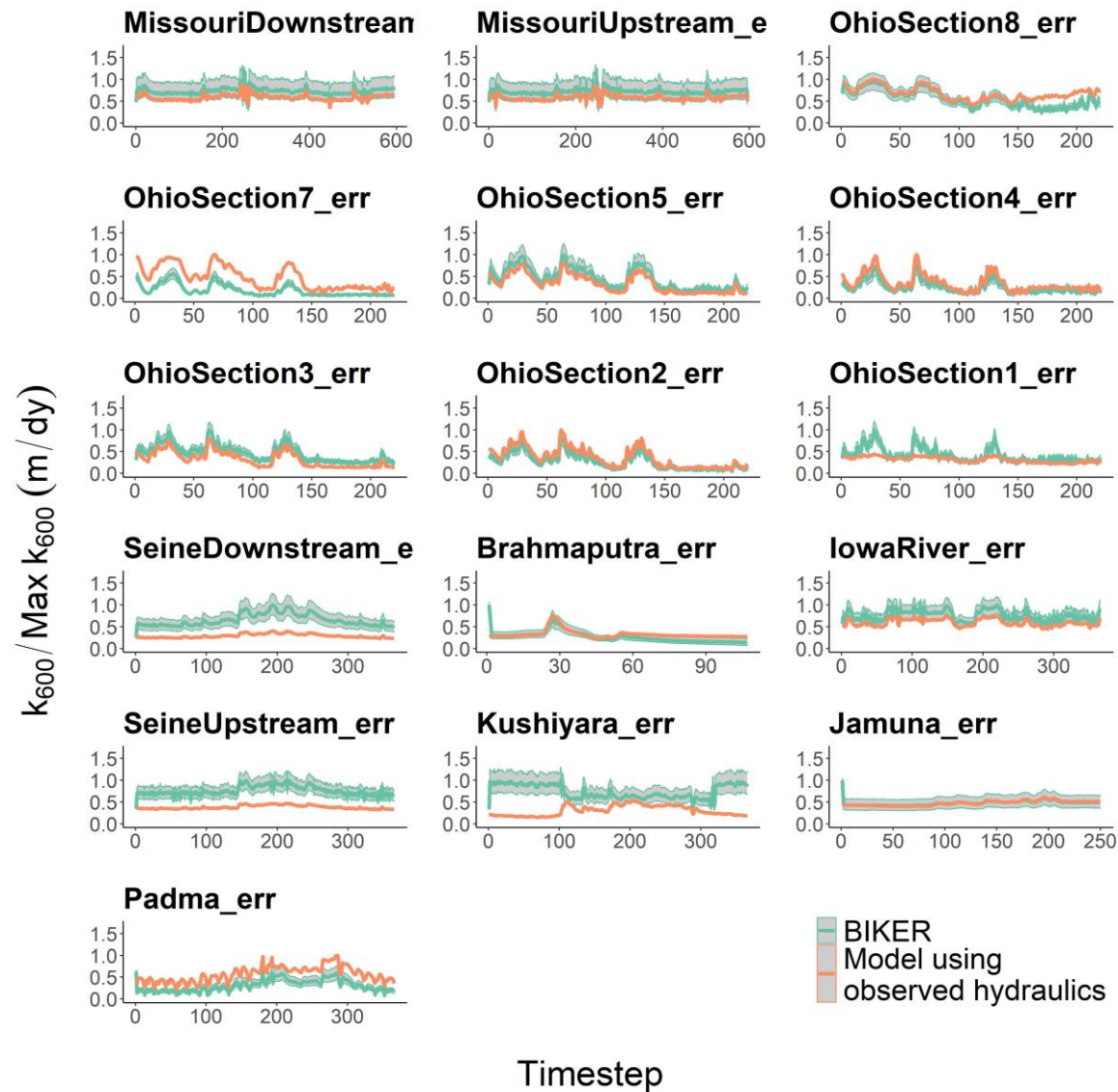
157   **Figure S5**

158

159   *Figure S5: Observed (orange) versus BIKER-inferred (green) timeseries of daily k_{600} for*

160   *16 rivers under the 'measurement-error' scenario. Green ribbon is BIKER posterior 95%*

161   *confidence intervals. Note that the y axis is normalized by maximum observed values to compare*

162   *across rivers.*

163   **Table S1**

164   *Table S1: Studies that gas exchange velocity measurements come from. 'Study' refers to*

165   *the paper from which these measurements were obtained by us. Any data wrangling was done by*

166   *those authors. 'Workers' refers to who actually made the measurements in the field. The Raymond*

167   *et al. (2012) dataset is itself a meta-analysis. Please see that paper for how those measurements*

168   *were collected, and see the 'Additional Studies' for the workers who actually collected the*

169   *measurements.*

Study	Workers	Additional studies
Ulseth et al. (2019)	Ulseth et al. (2019)	NA
Ulseth et al. (2019)	Hall & Madinger (2018)	NA
Ulseth et al. (2019)	Schelker et al. (2016)	NA
Ulseth et al. (2019)	Maurice et al. (2017)	NA
Ulseth et al. (2019)	Raymond et al. (2012)	Melching & Flores (1999); Bott, Montgomery, et al. (2006); Bott, Newbold, et al. (2006); Mulholland et al. (2001); Bernot et al. (2010); Tsivoglou & Wallace (1972)
Churchill et al. (1964)	Churchill et al. (1964)	NA
Owens et al. (1964)	Owens et al. (1964)	NA

170   **Table S2**

171   *Table S2: Details on the 3 literature models for CO_2 fluxes. See Text S5 for more details.*

Name	Depth equation	Velocity equation	Description	Reference
Brinkerhoff 2019	$D = 0.252Q^{0.388}$	$\bar{U} = 0.276Q^{0.164}$	104,624 measurements made across the United States at streamgauges	Brinkerhoff et al. (2019)
Raymond 2012	$D = 0.409Q^{0.294}$	$\bar{U} = 0.194Q^{0.285}$	1,026 measurements across the United States	Raymond et al. (2012)
Raymond 2013	$D = 0.409Q^{0.294}, D = 0.449Q^{0.37}$	$\bar{U} = 0.194Q^{0.285}, \bar{U} = 0.346Q^{0.120}$	Average of the Raymond 2012 equation and one using 9,811 measurements at US streamgauges	Raymond et al. (2013)

172   **References**

173   Altenau, E. H., Pavelsky, T. M., Durand, M. T., Yang, X., Frasson, R. P. de M., & Bendezu,

174   L. (2021). The Surface Water and Ocean Topography (SWOT) Mission River Database

175   (SWORD): A Global River Network for Satellite Data Products. *Water Resources Research*, *57*(7),

176   e2021WR030054. https://doi.org/10.1029/2021WR030054

177   Beaulieu, J. J., Shuster, W. D., & Rebholz, J. A. (2012). Controls on gas transfer velocities

178   in a large river. *Journal of Geophysical Research: Biogeosciences*, *117*(G2).

179   https://doi.org/10.1029/2011JG001794

180   Bernot, M. J., Sobota, D. J., Hall Jr, R. O., Mulholland, P. J., Dodds, W. K., Webster, J.

181   R., et al. (2010). Inter-regional comparison of land-use effects on stream metabolism. *Freshwater*

182   *Biology*, *55*(9), 1874–1890. https://doi.org/10.1111/j.1365-2427.2010.02422.x

183   Bott, T. L., Newbold, J. D., & Arscott, D. B. (2006). Ecosystem Metabolism in Piedmont

184   Streams: Reach Geomorphology Modulates the Influence of Riparian Vegetation. *Ecosystems*,

185   *9*(3), 398–421. https://doi.org/10.1007/s10021-005-0086-6

186   Bott, T. L., Montgomery, D. S., Newbold, J. D., Arscott, D. B., Dow, C. L., Aufdenkampe,

187   A. K., et al. (2006). Ecosystem metabolism in streams of the Catskill Mountains (Delaware and

188   Hudson River watersheds) and Lower Hudson Valley. *Journal of the North American*

189   *Benthological Society*, *25*(4), 1018–1044. https://doi.org/10.1899/0887-

190   3593(2006)025[1018:EMISOT]2.0.CO;2

191   Brinkerhoff, C. B., Gleason, C. J., & Ostendorf, D. W. (2019). Reconciling at-a-Station

192   and at-Many-Stations Hydraulic Geometry Through River-Wide Geomorphology. *Geophysical*

193   *Research Letters*, *46*(16), 9637–9647. https://doi.org/10.1029/2019GL084529

194   Brinkerhoff, C. B., Gleason, C. J., Feng, D., & Lin, P. (2020). Constraining Remote River

195   Discharge Estimation Using Reach-Scale Geomorphology. *Water Resources Research*, *56*(11),

196   e2020WR027949. https://doi.org/https://doi.org/10.1029/2020WR027949

197   Churchill, M. A., Elmore, H. L., & Buckingham, R. A. (1964). The Prediction of Stream

198   Reaeration Rates. In B. A. Southgate (Ed.), *Advances in Water Pollution Research* (pp. 89–136).

199   Pergamon. https://doi.org/10.1016/B978-1-4832-8391-3.50015-4

200   Durand, M. T., Gleason, C. J., Garambois, P. A., Bjerklie, D., Smith, L. C., Roux, H., et

201   al. (2016). An intercomparison of remote sensing river discharge estimation algorithms from

202   measurements of river height, width, and slope. *Water Resources Research*, *52*(6), 4527–4549.

203   https://doi.org/10.1002/2015WR018434

204   Frasson, R. P. de M., Durand, M. T., Larnier, K., Gleason, C., Andreadis, K. M.,

205   Hagemann, M., et al. (2021). Exploring the factors controlling the error characteristics of the

206   Surface Water and Ocean Topography mission discharge estimates. *Water Resources Research*,

207   *n/a*(n/a), e2020WR028519. https://doi.org/https://doi.org/10.1029/2020WR028519

208   Hagemann, M. W., Gleason, C. J., & Durand, M. T. (2017). BAM: Bayesian AMHG-

209   Manning Inference of Discharge Using Remotely Sensed Stream Width, Slope, and Height. *Water*

210   *Resources Research*, *53*(11), 9692–9707. https://doi.org/10.1002/2017WR021626

211   Hall, R. O., & Madinger, H. L. (2018). Use of argon to measure gas exchange in turbulent

212   mountain streams. *Biogeosciences*, *15*(10), 3085–3092. https://doi.org/10.5194/bg-15-3085-2018

213   Hoff, P. D. (2009). *A First Course in Bayesian Statistical Methods*. New York: Springer.

214   Maurice, L., Rawlins, B. G., Farr, G., Bell, R., & Gooddy, D. C. (2017). The influence of

215   flow and bed slope on gas transfer in steep streams and their implications for evasion of CO2.

216   *JOURNAL OF GEOPHYSICAL RESEARCH-BIOGEOSCIENCES*, *122*(11), 2862–2875.

217   https://doi.org/10.1002/2017JG004045

218   Melching, C. S., & Flores, H. E. (1999). Reaeration Equations Derived from U.S.

219   Geological Survey Database. *Journal of Environmental Engineering*, *125*(5), 407–414.

220   https://doi.org/10.1061/(ASCE)0733-9372(1999)125:5(407)

221   Mulholland, P. J., Fellows, C. S., Tank, J. L., Grimm, N. B., Webster, J. R., Hamilton, S.

222   K., et al. (2001). Inter-biome comparison of factors controlling stream metabolism. *Freshwater*

223   *Biology*, *46*(11), 1503–1517. https://doi.org/10.1046/j.1365-2427.2001.00773.x

224   Owens, M., Edwards, R. W., & Gibbs, J. W. (1964). Some reaeration studies in streams.

225   *Inter. J. Air Water Poll.*, *8*, 469–486. Retrieved from https://ci.nii.ac.jp/naid/10025707421/

226   Raymond, P. A., Zappa, C. J., Butman, D., Bott, T. L., Potter, J., Mulholland, P., et al.

227   (2012). Scaling the gas transfer velocity and hydraulic geometry in streams and small rivers.

228   *Limnology and Oceanography*, 41–53. https://doi.org/10.1215/21573689-

229   1597669@10.1002/(ISSN)1939-5590.MethaneVI

230   Raymond, P. A., Hartmann, J., Lauerwald, R., Sobek, S., McDonald, C., Hoover, M., et al.

231   (2013). Global carbon dioxide emissions from inland waters. *Nature*, *503*(7476), 355–359.

232   https://doi.org/10.1038/nature12760

233   Schelker, J., Singer, G. A., Ulseth, A. J., Hengsberger, S., & Battin, T. J. (2016). CO2

234   evasion from a steep, high gradient stream network: Importance of seasonal and diurnal variation

235   in aquatic pCO2 and gas transfer. *Limnology and Oceanography*, *61*(5), 1826–1838.

236   https://doi.org/https://doi.org/10.1002/lno.10339

237   Tsivoglou, E. C., & Wallace, J. R. (1972). *Characterization of Stream Reaeration*

238   *Capacity*. U.S. Government Printing Office.

239   Ulseth, A. J., Hall, R. O., Boix Canadell, M., Madinger, H. L., Niayifar, A., & Battin, T. J.

240   (2019). Distinct air–water gas exchange regimes in low- and high-energy streams. *Nature*

241   *Geoscience*, *12*(4), 259–263. https://doi.org/10.1038/s41561-019-0324-8